Journal of Biomolecular NMR, 5 (1995) 49–58
ESCOM

J-Bio NMR 223

Selectively ^{13}C-enriched DNA: Dynamics of the C1'-H1' vector in d(CGCAAATTTGCG)$_2$

Florence Gaudin[a], Françoise Paquet[a], Luc Chanteloup[a], Jean-Marie Beau[b], Nguyen T. Thuong[a] and Gérard Lancelot[a,*]

[a]*Centre de Biophysique Moléculaire, CNRS, 1A Avenue de la Recherche Scientifique, F-45071 Orléans, France*
[b]*Université d'Orléans, Laboratoire de Biochimie Structurale associé au CNRS, BP 6759, F-45067 Orléans, France*

Received 12 July 1994
Accepted 11 August 1994

Keywords: DNA dynamics; ^{13}C-labeled DNA; Internal motions of DNA; ^{13}C NMR

Summary

In order to examine the internal dynamic processes of the dodecamer d(CGCAAATTTGCG)$_2$, the ^{13}C-enriched oligonucleotide has been synthesized. The three central thymines were selectively ^{13}C-labeled at the C1' position and their spin-lattice relaxation parameters $R(C_Z)$, $R(C_{X,Y})$, $R(H_Z \rightarrow C_Z)$, $R(2H_ZC_Z)$, $R(2H_ZC_{X,Y})$ and $R(H_Z^S)$ were measured. Density functions were computed for two models of internal motions. Comparisons of the experimental data were made with the spin-lattice relaxation rates rather than with the density functions, whose values were altered by accumulation of the uncertainties of each relaxation rate measurement. The spin-lattice relaxation rates were computed with respect to the motions of the sugar around the C1'-N1 bond. A two-state jump model between the anti- and syn-conformations with P(anti)/P(syn) = 91/9 or a restricted rotation model with $\Delta\chi = 28°$ and an internal diffusion coefficient of 30×10^7 s^{-1} gave a good fit with the experimental data. Twist, tilt or roll base motions have little effect on $^{13}C1'$ NMR relaxation. Simulation of spin-relaxation rates with the data obtained at several temperatures between 7 and 32 °C, where the dodecamer is double stranded, shows that the internal motion amplitude is independent of the temperature within this range, as expected for internal motion. Using the strong correlation which exists in a B-DNA structure between the χ and δ angle, we suggest that the change in the glycosidic angle value should be indicative of a sugar puckering between the C1'-exo and C2'-endo conformations.

Introduction

Several studies have shown that DNA exhibits polymorphism and is commonly involved in a conformational equilibrium in solution. NMR relaxation experiments can, as a rule, provide a detailed description of nucleic acid dynamics. This is often accomplished using T_1, $T_{1\rho}$ and NOE experiments which are related to the spectral density functions describing such motions at a number of frequencies. These data depend on the global and internal dynamics of the macromolecule, as well as the distance between the nucleus under study and its surroundings. Several attempts to describe internal motions of the backbone (Hogan and Jardetzky, 1979,1980; Keepers and James, 1982), of sugar repuckering (Keepers and James, 1982; Borer et al., 1994) or of base-pair opening (Leroy et al., 1985; Gueron et al., 1987; Briki et al., 1991) have been published to date. Precise conclusions were, however, difficult to deduce from these studies because several motions imply a change in orientation and distances which must be simultaneously taken into account to reflect the experimental data. In order to facilitate determination of dynamics, a pair of nuclei having a fixed distance must be selected, such as H2'-H2" for the sugars or H5-H6 for the bases. Due to the rotation of the methyl group around the C-C bond of the thymine, the choice of the H6-CH_3 vector is more tedious. Moreover, the analysis of these data is greatly facilitated if only one neighbouring nucleus is involved in the relaxation process. Therefore, ^{13}C-^1H NMR is the best choice to investigate the dynamic process. In order to increase the low natural abundance of the isotope, selectively ^{13}C-labeled molecules are required.

*To whom correspondence should be addressed.

We present here an NMR investigation of the C1'-H1' dynamic processes in the oligonucleotide d(CGCAAATTTGCG)$_2$. Several studies have been devoted to the crystallographic structure of the oligonucleotide alone (Edwards et al., 1992) or complexed with drugs (Coll et al., 1987; Brown et al., 1992; Tabernero et al., 1993; Vega et al., 1994). Its crystallographic structure has been solved to 2.2 Å resolution (Edwards et al., 1992) and the helix was described as a right-handed B-DNA type. This conclusion is in agreement with the results of NMR studies of the oligonucleotide alone in solution (Gaudin, F. and Lancelot, G., unpublished data) or complexed with distamycin (Pelton and Wemmer, 1989). In order to investigate some aspects of the internal dynamics of B-DNA, the oligonucleotide d(CGCAAATTTGCG)$_2$, selectively ^{13}C-labeled on the three central thymine residues, was synthesized and rates of the six relaxation parameters were measured. We present models of internal motion which support the experimental data.

Materials and Methods

The natural oligonucleotide d(CGCAAATTTGCG) was purchased from Eurogentec (Seraing, Belgium) and purified by HPLC methods. The [1'-^{13}C]-dT was prepared by *N*-glycosylation in a Vorbrüggen-type procedure (trimethylsilyl-trifluoromethanesulfonate as a promoter, 1,2-dichloroethane as solvent) of the silylated nucleobases with [1'-^{13}C]-phenylsulfinyl-2,3,5-tri-*O*-benzoyl-β-D-ribofuranoside, available in four steps (77% overall yield) from commercial [1'-^{13}C]-D-ribose (99% ^{13}C-enriched, Centre d'Etudes Nucléaires, Saclay). The required 1'-^{13}C-labeled oligodeoxynucleotide was prepared on a Pharmacia automatic synthesizer via phosphoramidite chemistry using the classical unlabeled or [1'-^{13}C]-labeled deoxynucleotide 5'-*O*-dimethoxytrityl-3'-*O*-(β-cyanoethyl-*N,N*-diisopropylphosphoramidite) building block (Vorbrüggen et al., 1981; Robins et al., 1983; Sinha et al., 1983; Chanteloup and Beau, 1992). After deprotection, the oligodeoxynucleotide was purified by anion exchange chromatography on a mono Q-column (Pharmacia) and analyzed by reversed-phase HPLC.

NMR samples

Oligonucleotide solutions were passed through a chelex-100 column to remove paramagnetic impurities and adjusted to pH 7.0, then lyophilized from D_2O and dissolved in D_2O containing 0.1 M NaCl. The NMR samples (3 mM) were degased and were kept in sealed tubes.

NMR spectroscopy

NMR experiments were performed between 7 and 42 °C on a Bruker AMX-500 spectrometer and processed on an X32 computer. All data sets were recorded as 256 × 1024 real matrices. For each t_1 value, 64 scans were collected with a relaxation delay of 1.8 s between transients, except for $R(H_Z \rightarrow C_Z)$ measurements where the relaxation delay was 5 s. The matrix was zero-filled along the t_1 axis and multiplied in the F2 direction by a Gaussian function and in the F1 direction by a sinus function, shifted by π/4. The Fourier-transformed spectra were baseline corrected in both dimensions with a second-order polynomial. The cross-peak volumes were calculated with the integration routines of the UXNMR software package on the Bruker Aspect X32 workstation.

Relaxation rate measurements

The relaxation rates of $R(C_Z)$, $R(C_{X,Y})$, $R(H_Z \rightarrow C_Z)$, $R(2H_ZC_Z)$, $R(2H_ZC_{X,Y})$ and $R(H_Z^C)$ were measured following the pulse sequences described before (Kay et al., 1992; Peng and Wagner, 1992). Heteronuclear spin-lock and proton irradiation during the relaxation period were used in order to decouple the cross-relaxation pathways during the relaxation experiments, and to approach monoexponential behaviour as closely as possible (Boyd et al., 1990; Palmer et al., 1991; Peng and Wagner, 1992). T_1 and $T_{1\rho}$ curves were fitted as described in Fig. 1. In order to estimate accurately the heteronuclear NOE value, $R(H_Z \rightarrow C_Z)$ was measured for cross-relaxation delays of 800, 1200, 1600 and 2000 ms. The $R(2H_ZC_Z)$ value was fitted with 13 data points at 0, 20, 40, 60, 80, 100, 110, 140, 170, 200, 300, 400 and 600 ms. The $R(2H_ZC_{X,Y})$ value was fitted with 13 data points at 0, 0.52, 2.6, 13, 26, 39, 52, 65, 78, 91, 104, 130 and 156 ms. The $R(H_Z^C)$ value was fitted with 13 data points at 0, 10, 50, 100, 150, 200, 250, 300, 350, 400, 500, 600 and 800 ms.

Curve fitting was performed using a least-squares program (Lancelot, 1977) to minimize the value of χ^2, given by:

$$\chi^2 = \sum_{i=1}^{n} w_i \left[I_e(t_i) - I_c(t_i) \right]^2$$

In this equation, I_e and I_c are the experimental and calculated values at time t_i, w_i is the weight of the data and n is the number of time points recorded. w_i is in theory equal to $1/\sigma_i^2$, where σ_i is the uncertainty in the experimental data point i. By repeating the same experiment several hundred times, σ_i can be computed. Since this test is not practically feasible, we have estimated σ following two methods. First, w_i was taken equal to one for each data point. σ was then estimated for each experimental data point from the smaller χ^2 computed, and w_i taken as $|1/I_e(i) - I_c(i)|^2$. Uncertainties in the optimized parameters were obtained from the covariance matrix of the optimized model. By taking $w_i = 1$ for all i, the relaxation time uncertainties were overestimated, thus the optimized w_i led to an underestimation of uncertainties. This procedure has the advantage of restricting errors.

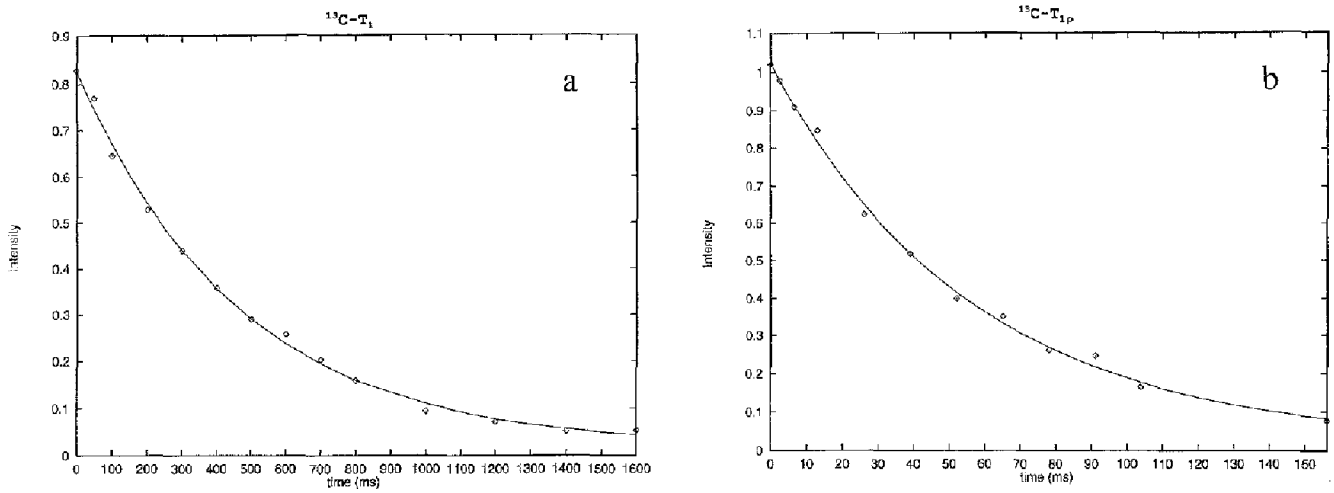

Fig. 1. Examples of relaxation curves resulting from T_1 (a) and $T_{1\rho}$ (b) experiments at 22 °C. (a) T_1 fit consisting of 14 points at 0, 50, 100, 200, 300, 400, 500, 600, 700, 800, 1000, 1200, 1400 and 1600 ms. The T_1 fitted value was 462 ± 20 ms in a 90% confidence interval; (b) $T_{1\rho}$ fit consisting of 12 points at 0, 2.6, 6.5, 13, 26, 39, 52, 65, 78, 91, 104 and 156 ms. The $T_{1\rho}$ fitted value was 49 ± 5.2 ms in a 90% confidence interval.

The second way to estimate w_i is to test the distribution of $I_e(i) - I_c(i)$ by running several experiments. A 300 data point set was examined and the distribution of errors established. Then, for typical values of the parameters I_1, I_2 and T, 500 data sets were generated by adding simulated errors E_i to theoretical points: $I(t_i) = I_1 + I_2 e^{-t/T}$. E_i values were chosen at random from the experimental distribution using Monte Carlo simulation. The statistical properties of the relaxation parameters were assumed to be equal to the properties of the experimental distribution. The computed uncertainty in the T_1 value was then given on a 90% confidence interval.

Typically, the adjustment of w_i leads to an uncertainty in the range 12–20 ms for a T_1 value of 462 ms; the Monte Carlo simulation gives uncertainties of ±13, ±20 and ±34 ms for confidence intervals of 75, 90 and 95%, respectively (Fig. 1). The high uncertainty value obtained at 95% (as compared to 90%) was induced by the small number of experimental data points (300) used to test the experimental error distribution.

Theory

The density function can be expressed as follows (Abragam, 1961):

$$J_q(\omega) = 2\int_0^\infty G_q(\tau) e^{-i\omega\tau} d\tau \qquad (1)$$

where the correlation function $G_q(\tau)$ is given by:

$$G_q(\tau) = p(\Omega_1)\, p(\Omega_1;\Omega_2,\tau)\, F^{(q)}(\Omega_1)\, F^{(q)}(\Omega_2) \qquad (2)$$

The functions $F(\Omega)$ are related to the spherical harmonic Y_l^m by:

$$F^{(0)} = -\sqrt{\frac{16\pi}{5}}\, Y_2^0$$

$$F^{(\pm 1)} = \pm\sqrt{\frac{8\pi}{15}}\, Y_2^{\pm 1} \qquad (3)$$

$$F^{(\pm 2)} = \pm\sqrt{\frac{32\pi}{15}}\, Y_2^{\pm 2}$$

$p(\Omega_1)$ is the probability to find the internuclear vector in the Ω_1 direction at time t and $p(\Omega_1,\Omega_2,\tau)$ is the conditional probability to find the internuclear vector in the Ω_2 direction at time $t + \tau$ if it was in the Ω_1 direction at time t.

The spherical harmonic $Y_l^m(\Omega_2)$ is related to $Y_l^m(\Omega_1)$ by:

$$Y_l^m(\Omega_2) = \sum_{m'=-l}^{l} Y_l^{m'}(\Omega_1)\, D^{*l}_{mm'}(\alpha,\beta,\gamma) \qquad (4)$$

where $D^l_{mm'}(\alpha,\beta,\gamma)$ are the Wigner matrix elements with the Euler angles α, β, γ (Rose, 1957) and Ω are the angular coordinates (θ,φ).

Combination of Eqs. 1–4 gives the relation:

$$J_q(\omega) = 2K_q \int_0^\infty p(\Omega_1)\, p(\Omega_1;\Omega_2,\tau) \sum_{m=-2}^{+2} \sum_{m'=-2}^{+2} D^2_{qm}(\Omega_1) D^2_{qm'}(\Omega_2) e^{-i\omega\tau} d\tau\, Y_l^m(\Omega_1)\, Y_l^{m'}(\Omega_2) \qquad (5)$$

with $K_0 = 16\pi/5$, $K_1 = 8\pi/15$ and $K_2 = 32\pi/15$.

When the internal motion is not correlated to the global tumbling motion of the cylinder, the expression of the density function can be written as the sum of the relaxation processes generated by the global and internal motions. In one of our models, the internuclear vector can jump between two sites inside a rigid cylinder. The density functions can then be written as follows:

$$J_q(\omega) = K_q \sum_{n=-2}^{+2} \left(\frac{2Y_2^n(\Omega_1)Y_2^{*n}(\Omega_2)}{r_1^3 r_2^3} p_1^{eq} p_2^{eq} + \frac{\left|Y_2^n(\Omega_1)\right|^2}{r_1^6} (p_1^{eq})^2 + \frac{\left|Y_2^n(\Omega_2)\right|^2}{r_2^6} (p_2^{eq})^2 \right) \frac{\tau_{n0}}{1+\omega^2\tau_{n0}^2}$$

$$+ K_m \sum_{n=-2}^{+2} \left(\frac{2Y_2^n(\Omega_1)Y_2^{*n}}{r_1^3 r_2^3} p_1^{eq} c_{22} + \frac{\left|Y_2^n(\Omega_1)\right|^2}{r_1^6} p_1^{eq} c_{12} + \frac{\left|Y_2^n(\Omega_2)\right|^2}{r_2^6} p_1^{eq} p_2^{eq} \right) \frac{\tau_{n1}}{1+\omega^2\tau_{n1}^2} \quad (6)$$

where (Ω_1) and (Ω_2) represent the Euler angles which describe the two positions of the vector versus a frame fixed to the molecule.

When the overall motion can be modeled as the anisotropic motion of a cylinder,

$$\tau_{n0}^{-1} = 6D_{\perp} + n^2(D_{\parallel} - D_{\perp})$$
$$\tau_{n1}^{-1} = \tau_{n0}^{-1} + \lambda \quad (7)$$

$D_{\parallel}$ and $D_{\perp}$ are the longitudinal and transversal diffusion coefficients.

The conditional probabilities have been computed by the method of Wittebort and Szabo (1978) using the velocity matrix [K]. For a two-state jump model:

$$\begin{bmatrix} \mathbf{p}^0(1,\mathbf{t};1,0) \\ \mathbf{p}^0(2,\mathbf{t};1,0) \end{bmatrix} = [\mathbf{K}] \begin{bmatrix} \mathbf{p}(1,\mathbf{t};1,0) \\ \mathbf{p}(2,\mathbf{t};1,0) \end{bmatrix} \quad (8)$$

with

$$\mathbf{K} = \begin{bmatrix} -\mathbf{K}_1 & +\mathbf{K}_2 \\ +\mathbf{K}_1 & -\mathbf{K}_2 \end{bmatrix}$$

and $c_{12} = k_1/(k_1 + k_2)$, $c_{22} = -k_1/(k_1 + k_2)$, $p_1^{eq} = k_2/(k_1 + k_2)$, $p_2^{eq} = k_1/(k_1 + k_2)$ and $\lambda = k_1 + k_2$.

p_1^{eq} and p_2^{eq} represent the equilibrium populations of the two sites and c_{12}, c_{22} and λ are the eigenvectors and the eigenvalues of the velocity matrix [K] which describes the transition between the two states. Ω_1 and Ω_2 are then the azimuthal angles θ of the vector $^{13}C1'$-$^1H1'$ in the two conformations; for example, in the syn and anti conformations of the base, $\theta_1 = 65°$ and $\theta_2 = 125°$, respectively.

The second model is related to a restricted diffusion of a vector between the angle $\theta + \Delta\theta$. The expressions of $p(\Omega_1,\Omega_2,\tau)$ published by Wittebort and Szabo (1978) were used. $J(\omega)$ was computed from:

$$J_q(\omega) = K_q \sum_{n=-2}^{+2} \left|Y_2^n(\theta)\right|^2 \sum_{l=0}^{\infty} \Gamma_{ln}(\theta,\Delta\theta) \frac{\tau_n}{1+\omega^2\tau_n^2} \quad (9)$$

$$\tau_n^{-1} = 6D_{\perp} + n^2(D_{\parallel} - D_{\perp}) + D \quad (10)$$

$$D = \frac{D_i n^2 \pi^2}{4\Delta\theta^2} \quad (11)$$

where D_i is the internal diffusion coefficient of the vector between the angle θ and $\theta + \Delta\theta$. The series expression $\Gamma_{ln}(\theta,\Delta\theta)$ converges rapidly and only the first 10 terms were required. Its expression is given by relation 3.12 in the paper of Wittebort and Szabo (1978).

Results

^{13}C spin-lattice relaxation rate measurements

The expanded $^1H1'$-$^{13}C1'$ region of the HSQC spectrum of the ^{13}C-labeled oligonucleotide shows three strong ^{13}C-^1H connectivities, corresponding to the ^{13}C-labeled central thymines (not shown). Their assignments were made using the already assigned H1' resonances and verified in an HMQC-NOESY spectrum (Lancelot et al., 1993). In order to obtain information on the presence of internal motion of the vectors C1'-H1', the spectral density functions of rotational motions can be mapped as proposed by Peng and Wagner (1992).

The relaxation rates $R(C_Z)$, $R(C_{X,Y})$ and $R(H_Z \rightarrow C_Z)$ are a linear combination of five density functions. In order to compute them in this under-dimensioned system, $J(\omega_H - \omega_C)$ and $J(\omega_H + \omega_C)$ can be approximated as $J(\omega_H)$. The resulting computed density functions are given in Table 1. Another way to compute the density functions is to measure three more relaxation rates: $R(2H_ZC_Z)$, $R(2H_ZC_{X,Y})$ and $R(H_Z^C)$ (Peng and Wagner, 1992). In principle, the six relaxation rates can be expressed as a system of linear equations with six unknown parameters: $J(0)$, $J(\omega_C)$, $J(\omega_H)$, $J(\omega_H - \omega_C)$, $J(\omega_H + \omega_C)$ and $\rho_H c^H$. The last term represents the spin-lattice relaxation rate of the H1' proton due to other protons. It consists of spectral density functions J which describe the motion of vectors joining the various H-H proton spin pairs. For the H1' proton, these vectors can be approximated by H1'-H2", whose length (2.3 Å) is almost independent of the conformation of the sugar and which is shorter than the other proton–proton distances (H1'-H6 = 3.6–3.8 Å, H1'-H2' = 3.1 Å, H1'-H3' = 3.8 Å, H1'-H4' = 3.1 Å). The relaxation of the nonequilibrium H_Z^C magnetization can then be approximated by an exponential decay to yield $R(H_Z^C)$. The corresponding computed density functions are given in Table 1. Unfortunately, uncertainties in the relaxation rates induce large absolute errors in the different density functions. For example, $J(\omega_H)$ is computed from a combination of five relaxation rates:

$$J(\omega_H) = \frac{1}{12d}(-R(C_Z) + 2R(C_{XY}) - 2R(2H_ZC_{XY}) + R(2H_ZC_Z) + R(H_Z^C)) \quad (12)$$

In this expression $R(C_{X,Y})$ and $R(2H_ZC_{X,Y})$ are in the range $20 \pm 1.9\ s^{-1}$, with an uncertainty much larger than the resulting value of $12.d.J(\omega_H)$ which is 0.58 s ($d = 6 \times 10^9\ s^{-2}$ for $r_{C-H} = 1.07$ Å and $J(\omega_H) = 0.008 \times 10^{-9}$ s from Table 1). Thus, an important uncertainty affects the J value, as shown in Table 1: $J(\omega_H) = 0.022 \pm 0.075 \times 10^{-9}$ s. Consequently, although mapping the spectral density functions gives information about the presence of internal motion for a given vector and the time scale on which this motion occurs, it cannot be used here to describe the motion that occurs. Another way to test the internal motions model is to compute directly the relaxation rates and to compare them with the experimental values. This method avoids the accumulation of uncertainties of the different experimental relaxation rates.

The relaxation rates computed with a global correlation time of 4.80 ns, an effective correlation time less than or equal to 16 ps and a parameter order of 0.831 are in better agreement with the experimental data than the computed values using the tumbling rigid sphere model (Table 2). Although this Lipari–Szabo relation (Lipari and Szabo, 1982a,b) was model independent and the global tumbling motion could be described by only one correlation time, the computed parameters give evidence of rapid internal motion. A more realistic model has to take into account the cylindric global shape of the dodecamer. It can be modeled by a cylinder with a length of 12 times 3.4 Å (L = 40.8 Å) and a diameter D of 20.5 Å (Eimer et al., 1990). Then, the simulated NMR cross-relaxation monitors the reorientation of a cylindrical molecule about its long and short molecular symmetry axes. Tirado and Garcia de la Torre (1979,1980) gave the expression for the translational $D_\parallel$ and rotational $D_\perp$ diffusion coefficients of rod-like molecules for $2 \leq L/D \leq 30$. We have used these relations to compute $D_\parallel/D_\perp = 2.2$ and the final diffusion coefficient values were adjusted to give the best fit with the experimental data. Three correlation times contribute to the simulated effective correlation time for a vector (see Eq. 7) whose orientation is determined by its azimuthal θ angle with the long axis of the cylinder (Table 2).

Models of relaxation processes

A careful computation of the spin-lattice relaxation rates of C1' must consider all possible orientations of the vector C1'-H1'. These motions are the result of correlated motions of the base and of the motion of the sugar relative to the base. First, we computed spin-lattice relaxation rates by taking into account the rotation of the sugar with respect to the C1'-N1 bond.

Crystallographic (Saenger, 1984) and NMR data (Wüthrich, 1986) indicate that in oligonucleotides, two stable conformations, anti and syn, are present. Furthermore, Drew et al. (1981) reported that in many cases, the deoxyribose ring appears to be rocking about the C1'-N bond. Consequently, the internal dynamic effect of the C1'-H1' vector was simulated using two internal motion models. The first one describes the effect of a jump be-

TABLE 1
EXPERIMENTAL AND THEORETICAL DETERMINATION OF SPECTRAL DENSITY FUNCTIONS

	J(0)	$J(\omega_C)$	$J(\omega_H - \omega_C)$	$J(\omega_H)$	$J(\omega_H + \omega_C)$	$\rho_H{}^{C^H}$
Experimental						
(a)	1.45 ± 0.18	0.110 ± 0.005	0.0038	0.0038	0.0038	
(b)	1.48 ± 0.20	0.082 ± 0.012	0.047 ± 0.019	0.022 ± 0.075	0.011 ± 0.003	1.9 ± 1.3
Theoretical						
(c)	1.44	0.160	0.020	0.011	0.0070	
(d)	1.54	0.160	0.019	0.011	0.0070	
(e)	1.60	0.106	0.013	0.008	0.0056	
(f)	1.59	0.106	0.013	0.008	0.0053	3.05
(g)	1.59	0.105	0.013	0.008	0.0052	3.05

The experimental J(ω) were calculated (in 10^{-9} s) using:
(a) The spin relaxation rates $R(C_{X,Y})$, $R(C_Z)$ and $R(H_Z \rightarrow C_Z)$ and the approximation $J(\omega_H - \omega_C) = J(\omega_H) = J(\omega_H + \omega_C)$. Due to this approximation the uncertainties in $J(\omega_H - \omega_C)$, $J(\omega_H)$ and $J(\omega_H + \omega_C)$ are not indicated.
(b) The six spin relaxation rates.
The theoretical J(ω) were calculated, using the relation $J(\omega) = 2/5\ \tau/(1 + \omega^2\tau^2)$:
(c) For a tumbling rigid sphere, $\tau = 3.61$ ns.
(d) For a tumbling rigid cylinder: $D_\parallel = 6.69 \times 10^7\ s^{-1}$; $D_\perp = 3.04 \times 10^7\ s^{-1}$; $\theta = 65°$; $J(\omega) = 1/4\ (3\cos^2\theta - 1)j(\tau_1) + 3\cos^2\theta \sin^2\theta\, j(\tau_2) + 3/4 \sin^4\theta\, j(\tau_3)$; $j(\tau) = 2/5\ \tau/(1 + \omega^2\tau^2)$; $\tau_1^{-1} = 6D_\parallel$; $\tau_2^{-1} = D_\parallel + 5D_\perp$; $\tau_3^{-1} = 4D_\parallel + 2D_\perp$.
(e) By the Lipari–Szabo expression: $\tau_g = 4.80$ ns; $\tau_i = 16$ ps; $S^2 = 0.831$; $J(\omega) = 2/5\ (S^2\tau_g/(1 + \omega^2\tau_g^2) + (1 - S^2)\tau_i/(1 + \omega^2\tau_i^2)$.
(f) For a jump between two states inside a tumbling cylinder: $D_\parallel = 5.09 \times 10^7\ s^{-1}$; $D_\perp = 2.31 \times 10^7\ s^{-1}$; $k_1 = 0.9\ ps^{-1}$; $k_2 = 9.1\ ps^{-1}$; $\theta_1 = 65°$; $\theta_2 = 125°$.
(g) For a restricted rotation model: $D_\parallel = 4.79 \times 10^7\ s^{-1}$; $D_\perp = 2.18 \times 10^7\ s^{-1}$; $D_i = 30 \times 10^7\ s^{-1}$; $\Delta\chi = 28°$.
The chemical shift anisotropy = −40 ppm for all models.

TABLE 2
EXPERIMENTAL AND COMPUTED SPIN-LATTICE RELAXATION RATES

Relaxation rates (s^{-1})	$R(C_{X,Y})$	$R(C_Z)$	$R(H_Z \rightarrow C_Z)$	$R(2H_ZC_{X,Y})$	$R(2H_ZC_Z)$	$R(H_Z^C)$
Experimental	20.4 ± 1.9	2.16 ± 0.09	0.119 ± 0.017	23.1 ± 1.9	4.96 ± 0.2	4.16 ± 0.4
Rigid sphere (a)	20.4	3.26	0.139	23.3	6.16	3.65
Rigid cylinder (b)	20.4	3.18	0.137	23.0	5.91	3.47
Lipari–Szabo (c)	20.4	2.16	0.11	23.1	4.86	3.12
Jump between two sites (d)	20.4	2.18	0.110	23.3	5.10	3.46
Restricted rotation model (e)	20.4	2.17	0.110	23.3	5.09	3.46
Contribution of CSA (f)	0.4	0.03	0	0.4	0.03	0

The measured ^{13}C relaxation rates and NOEs were the same for the three thymines T_7, T_8, T_9 within experimental error. Averages at 22 °C were: $T_{1\rho} = 49 \pm 5.2$ ms, $T_1 = 462 \pm 20$ ms, NOE = 1.2 ± 0.1, $R^{-1}(2H_ZC_{X,Y}) = 43.3 \pm 3.6$ ms, $R^{-1}(2H_ZC_Z) = 201 \pm 8$ ms, $R^{-1}(H_Z^C) = 240 \pm 23$ ms. Small variations from the average, within experimental uncertainty, were detected for the three thymines. $T_{1\rho}$ was measured with a ^{13}C radio frequency offset lower than 20 Hz. When the ^{13}C carrier frequency differed from the $^{13}C1'$ frequency by more than 1 ppm the accuracy of $R(C_{X,Y})$ was improved by correcting the effective spin-lock field using Eq. 19 of the paper by Peng et al. (1991).
The computations were made using:
(a) The model of a tumbling rigid sphere with $\tau_g = 3.61$ ns.
(b) A tumbling rigid cylinder with $D_\parallel = 6.69 \times 10^7\ s^{-1}$; $D_\perp = 3.04 \times 10^7\ s^{-1}$.
(c) The Lipari–Szabo approximation with $\tau_g = 4.80 \pm 0.01$ ns; $\tau_i = 16$ ps; $S^2 = 0.831 \pm 0.008$.
(d) A two-state jump model inside a rod-like cylinder; $\theta_1 = 65°$, $\theta_2 = 125°$ with $D_\parallel = 5.09 \times 10^7\ s^{-1}$; $D_\perp = 2.31 \times 10^7\ s^{-1}$; $k_1 = 0.9\ ps^{-1}$; $k_2 = 9.1\ ps^{-1}$.
(e) A restricted rotation model with $D_\parallel = 4.79 \times 10^7\ s^{-1}$; $D_\perp = 2.18 \times 10^7\ s^{-1}$; $D_i = 30 \times 10^7\ s^{-1}$; $\Delta\chi = 28°$.
(f) The $^{13}C1'$ chemical shift anisotropy has been taken as −40 ppm, in agreement with known values for ethanol $\Delta\sigma = -28.5$ ppm (Pines et al., 1972), diethyl ether $\Delta\sigma = -45.5$ ppm (Pines et al., 1972), L-threonine $\Delta\sigma = -26.95$ ppm (Janes, 1983), L-serine $\Delta\sigma = -35.5$ ppm (Naito, 1983). The contribution to the CSA of the various relaxation times is given for the two-state jump model with the parameters (d) or for the restricted rotation model with the parameters (e).
For all models, $\rho_H c^H = 3.05\ s^{-1}$.

tween two stable conformations. The second model allows a restricted diffusion around the glycosidic bond of the C1'-H1' vector between the angles $\chi \pm \Delta\chi$. In the jump model, one of the two states θ_1 was fixed using the direction of the vector C1'-H1' in a canonical B-type structure of the dodecamer. The spin-lattice relaxation rates computed for an anti population and a θ_2 value of 125°, corresponding to a syn conformation of the torsional glycosidic angle, are given in Table 2. The best fit for $R(C_{X,Y})$, $R(C_Z)$ and $R(H_Z \rightarrow C_Z)$ was estimated for an anti population of 91% (Table 2). The computed $R(2H_ZC_{X,Y})$, $R(2H_ZC_Z)$ values were also found to be in agreement with the experimental data. The computed $R(H_Z^C)$ value (3.31 s^{-1}) was found to lie outside the experimental range of 3.76–4.56 s^{-1}. This discrepancy is explained by the fact that the experimental $R(H_Z^C)$ value was deduced from a monoexponential analysis of the data curve, whereas this relaxation process is highly multiexponential due to the number of protons surrounding the H1' proton.

Using the restricted rotation model, the best fit was obtained for a variation of the glycosidic angle $\Delta\chi$ of 28° (Table 2). The relative contribution of chemical shift anisotropy to the various relaxation times was less than 2% (Table 2).

Influence of roll, tilt and twist motions of the bases on spin relaxation rates

The influence of roll, tilt and twist motions of the bases on $^{13}C1'$ spin-lattice relaxation rates was investigated using a two-restricted rotation model. The first restricted rotation describes the local motion of the bases around the suitable diffusion axis. This axis was taken perpendicular to the base plane for twist motions, or in the base plane for roll (C6(dT)-C8(dA)) or tilt (pseudo-dyad axis) motions. The second restricted rotation describes the motion of the C1'-H1' vector around the glycosidic bond. The resulting spin-lattice relaxation rates were computed for several amplitudes and diffusion coef-

TABLE 3
CONTRIBUTION OF TWIST, TILT AND ROLL BASE MOTIONS TO SPIN-LATTICE RELAXATION RATES

	$\Delta\theta$	$R(C_{X,Y})$	$R(C_Z)$	$R(H_Z \rightarrow C_Z)$	$R(2H_ZC_{X,Y})$	$R(2H_ZC_Z)$	$R(H_Z^C)$
Twist	±5°	20.29	2.15	0.108	23.22	5.09	3.47
(a)	±10°	19.86	2.09	0.106	22.79	5.04	3.46
Tilt or roll	±5°	20.29	2.15	0.108	23.22	5.10	3.48
(b)	±10°	19.85	2.12	0.106	22.78	5.06	3.47
(c)		20.40	2.17	0.110	23.3	5.11	3.48

$\Delta\theta$ is the amplitude of the motion.
(a) Twist motion ($\Delta\theta$) and restricted rotation around the C1'-N bond with $\Delta\chi = 28°$.
(b) Tilt or roll motion and restricted rotation around the C1'-N bond with $\Delta\chi = 28°$.
(c) Best fit of spin-lattice relaxation rates computed with a restricted rotation model: twist ±5°, tilt ±5°, roll ±5°, $\Delta\chi = 25°$, $D_i = 30 \times 10^7\ s^{-1}$.

ficients of the base motion (Table 3). A comparison with the results of Table 1, which take into account only the rotation about the glycosidic bond, shows that small amplitudes (5–10°) of roll, tilt or twist motions induce weak variations in the spin-lattice relaxation rates. Moreover, for these amplitudes the computed rates were almost insensitive to the diffusion coefficient in the range of $0.3–300 \times 10^7$ s^{-1}.

Effect of temperature on internal motions

Under our experimental conditions, the T_m of the dodecamer was measured to be 55 °C. The observed variation of base proton chemical shifts showed that more than 95% of the strands were self-associated below 32 °C. In order to examine the temperature effect on internal motions, the spin-lattice relaxation rates were measured at several temperatures. Raising the temperature from 7 to 32 °C decreased the $R(C_{X,Y})$ value by 68% and increased the $R(C_Z)$ value by 149%. The internal motion parameters obtained at 32 °C fitted well the experimental data obtained at 7 °C using the two-state jump model or the restricted rotation model (Table 4) when the $D_\parallel$ and $D_\perp$ values were increased by 196%. This demonstrates that lowering the temperature has the well-known effect of increasing the viscosity of the DNA solution, but the amplitude of the internal motions is not affected by this 25 °C change. The diffusion coefficient of these motions is equal to about 10 times the global diffusion coefficient of the oligonucleotide. These data are in agreement with the expected low energy barriers for internal motions and represent a good test for the validity of our models. Above 32 °C, the two strands of the oligonucleotide were not completely associated and fitting data with the internal motion model inside a cylinder failed, as shown in Table 4.

Mapping of spectral density functions using relaxation measurements

When models of internal motions are available, a comparison of computed spin-lattice relaxation rates with the experimental data is the best way to test the validity of the assumptions. Unfortunately, internal dynamics can be the result of numerous internal motions and the map of spectral density functions can then be very useful for obtaining information on internal motions, despite the complexity of the physical system.

On the one hand, the approximation $J(\omega_H) = J(\omega_H \pm \omega_C)$ is based on the fact that $J(\omega_H)$ slowly varies with the frequency. In fact, our data (Table 1) show that $J(\omega_H - \omega_C)$ is 1.5 times higher than $J(\omega_H)$ and that $J(\omega_H)$ is also about 1.5 times higher than $J(\omega_H + \omega_C)$. Consequently, the computed $J(\omega_H)$ and $J(\omega_H \pm \omega_C)$ values are underestimated by this assumption.

On the other hand, the $J(\omega_H)$ values deduced from the six relaxation rates contain errors as a result of the analysis of $R(H_Z^C)$ data. Their decrease with the relaxation period was analyzed as monoexponential behaviour, but several protons participate in the H1'→H magnetization transfer. Although the H1'→H2" transfer is more efficient, numerous other ways exist, such as H1'→H8, H1'→H2', H1'→H3' and H1'→H4' transfers. Fitting of the $R(H_Z^C)$ data, using a combination of several exponentials, failed because good fits were obtained with different parameters. Consequently, the computed $R(H_Z^C)$ value was over-

TABLE 4
EXPERIMENTAL (a) AND SIMULATED VALUES OF SPIN-LATTICE RELAXATION RATES FOR THE TWO-STATE JUMP MODEL (b) AND THE RESTRICTED ROTATION MODEL (c) AT SEVERAL TEMPERATURES

T (°C)	Model	$D_\parallel$ (10^7 s^{-1})	$D_\perp$ (10^7 s^{-1})	k_1 (ps^{-1})[a] or D_i (10^7 s^{-1})[b]	k_2 (ps^{-1})[a] or $\Delta\chi$[b]	$R(C_{X,Y})$ (s^{-1})	$R(C_X)$ (s^{-1})	$R(H_Z \rightarrow C_Z)$ (s^{-1})
7	(a)					38.0 ± 3.5	1.06 ± 0.04	0.074 ± 0.010
	(b)	2.40	1.09	1.2	8.8	38.0	1.06	0.068
	(c)	2.38	1.08	30	30	38.0	1.14	0.071
12	(a)					29.0 ± 2.7	1.54 ± 0.06	0.081 ± 0.011
	(b)	3.48	1.57	0.9	9.1	29.0	1.56	0.082
	(c)	3.27	1.49	30	28	29.0	1.55	0.082
22	(a)					20.4 ± 1.9	2.16 ± 0.09	0.119 ± 0.017
	(b)	5.09	2.31	0.9	9.1	20.4	2.18	0.110
	(c)	4.79	2.18	30	28	20.4	2.17	0.110
32	(a)					14.2 ± 1.3	2.64 ± 0.11	0.152 ± 0.021
	(b)	7.10	3.23	1.2	8.8	14.2	2.71	0.145
	(c)	7.07	3.21	30	30	14.2	2.88	0.154
42	(a)					12.1 ± 1.1	2.94 ± 0.12	0.159 ± 0.022
	(b)	8.14	3.70	1.4	8.6	12.1	2.88	0.161
	(c)	7.90	3.59	30	34	12.1	2.97	0.178

(a) = experimental; (b) = jump between two sites; (c) restricted rotation model.
[a] k_1 and k_2 are exchange rates for the two-state jump model (b).
[b] $\Delta\chi$ and D_i are the angular fluctuation around the C1'-N bond and the internal diffusion coefficient for the restricted rotation model (c), respectively.

estimated and the resulting $J(\omega_H)$, $J(\omega_H \pm \omega_C)$ values as well.

To minimize the systematic errors introduced by the two methods, we propose, when internal motion models are not available, to evaluate $J(\omega_H)$ by averaging the two computed sets of data. When the models can be used, measurements of the three relaxation rates $R(C_{X,Y})$, $R(C_Z)$ and $R(H_Z \rightarrow C_Z)$ are sufficient to investigate the internal dynamic process.

Discussion

A good fit of the $R(C_{X,Y})$, $R(C_Z)$, $R(H_Z \rightarrow C_Z)$, $R(2H_ZC_{X,Y})$ and $R(2H_ZC_Z)$ values has been obtained using a two-state jump model between the anti and syn conformations, with P(anti)/P(syn) = 91/9 and an internal correlation time of 10 ps, or a restricted rotation model around the glycosidic bond with $\Delta\chi = 28°$ and a diffusion coefficient of 30×10^7 s^{-1}. The 'effective internal correlation time' in the range of 10 ps is in agreement with the value estimated by Borer et al. (1994) for sugar and base (30–300 ps) and with the value computed by Briki and Genest (1993) for the C1'-N1 vector (τ = 17.4 ps). The amplitudes of the motions are in agreement with the generalized order parameters ($S^2 = 0.92$ for H5-H6 and $S^2 = 0.90$ for H6-H1') calculated from molecular dynamics simulations on the DNA octamer d(GCGTTGCG)-d(CGCAACGC) (Koning et al., 1991) and with the data of Withka et al. (1992) who computed a ±18° azimuthal angle change of the H6-H1' vector around an average anti conformation for the dC_3 residue using a 200 ps dynamics trajectory for the dodecamer $d(CGCGAATTCGCG)_2$. Similarly, Briki (1993) computed a total variation of the χ angle in the range 30–40° around an average anti conformation for the different residues of the octamer $d(CTGATCAG)_2$. More recently, McConnell et al. (1994) reported a 1 ns MD run on the $d(CGCGAATTCGCG)_2$ duplex, complexed to the restriction enzyme EcoRI endonuclease. They reported that the oligonucleotide undergoes a distinct transition to a new form after 300 ps. A fast (1.5 ps) reversible base-pair opening event was observed at the dT_7 step. On the basis on these short dynamics trajectories, we cannot rule out that a restricted rotation around an anti conformation of the C1'-H1' bond and a jump between two conformations coexist in DNA. In principle, the H6-H1' NOE, whose distance is a function of the χ glycosidic angle value, should discriminate a jump between the anti and syn conformations from a restricted diffusion around a glycosidic bond. Unfortunately, this NOE depends on the orientation of the interproton vector azimuthal angle. Drew et al. (1981) reported a 50° dispersion of the χ angle along the sequence of the dodecamer. A variation of the glycosidic angle from 30° to 50° induces a 6 to 12% variation of the H6-H1' NOE. Using the two-state jump model between an anti conformation (r(H6-H1') = 3.7 Å) and a syn conformation (r(H6-H1') = 3.0 Å) and the exchange rates determined in Table 2, we have computed a 15% decrease of the H6-H1' NOE. Comparing the NOE changes obtained for different orientations or different fluctuations of the interproton vector orientation, we conclude that the H6-H1' NOE variations cannot be used to discriminate between the two-state jump model and the restricted rotation model. Attempts to decide between the two proposed internal motion models are hazardous at this time. A combination of these two types of motions could be taken into consideration.

Local motions of bases can change the value of the computed dynamic parameters. The amplitude of the base plane motions has been measured using different spectroscopic methods. By analyzing experimental data of fluorescence polarization of ethidium bromide–DNA complexes, Genest and Wahl (1978) reported that the base motions have a correlation time smaller than 1 ns and an amplitude of 10.5° at 20 °C. Combining these data with molecular dynamics studies, Briki and Genest (1993) analyzed the data in terms of rotational motions of the bases leading to a base-pair opening process, and not in terms of tilt or roll of the bases. From fluorescence polarization anisotropy and reduced linear dichroism data, Schurr and Fujimoto (1988) estimated the local internal motion of ethidium dye in DNA to be 6.9°–8°. They analyzed the NMR relaxation data reported by Early and Kearns (1979) for imino protons and estimated an amplitude of local base motions of 12°. Hogan and Jardetzky (1979,1980) computed a local motion of bases of ±20° with an internal correlation time of 1 ns by analyzing T_1, NOE and line width data of $^{13}C8$ and $^{13}C6$ resonances in a 260-base pair DNA fragment.

Running a 140 ps dynamics trajectory for $d(CGCGAATTCGCG)_2$, Swaminathan et al. (1991) reported amplitudes of roll and tilt of about ±5° around the average values. On the basis of all these data, we estimated the angular fluctuation of the base at about ±5°. A restricted rotation model indicated that such amplitudes of twist, roll or tilt motions induce a 1% NOE value variation in the H5-H6 NOE of cytosines. Conjugated motions such as twist, roll and tilt, each at ±5° amplitude and with restricted rotation around the glycosidic bond, were computed using a restricted rotation model. The best fit of the spin-lattice relaxation rates was obtained for a restricted rotation around a glycosidic bond of ±25° and a diffusion coefficient of 30×10^7 s^{-1}.

Such a fluctuation of the glycosidic angle induces coupled motions of the backbone and sugar. Fratini et al. (1982) have shown that the most fundamental aspects of B-DNA structure are the strong correlation between the glycosidic C1'-N angle χ and the main-chain torsion angle δ (C5'-C4'-C3'-O3') and the relationship between the latter angle and the sugar ring pucker. This correlation has

been reproduced in MD simulations on the duplex d(GTATAATG)•d(CATTATAC) (Schmitz et al., 1992). Using the relation $\delta = 309° + 1.59\chi_0$, obtained from crystallographic data on the oligonucleotide d(CGCGAATT-^{Br}CGCG)$_2$, a change of χ equal to ±20° will induce a ±32° change of δ. This variation corresponds roughly to a transition between the C1'-exo and the C2'-endo conformations. We suggest that the rotation around the C1'-N bond should reflect the fluctuation of the sugar puckering.

Conclusions

Experimental spin-lattice relaxation rates could be simulated well by computing the effect of local motions of the vector C1'-H1' on the density functions. Assuming no correlation between the global and internal motions of DNA, we have presented straightforward models for the internal mobility of the base pairs and of the sugars relative to the bases in DNA. These models fit the experimental data well and elucidate important relationships between the magnetic fluctuations detected by NMR on the C1' nucleus and the motional fluctuations. Motional models which entail DNA base tilt, roll and twist have little effect (less than 10%) on ^{1}H-^{1}H NOE values. Although the models support experimental data at several temperatures, the correlation effects between the internal motions and bending of the global shape of DNA cannot be excluded. Moreover, the spin-lattice relaxation rates are a function of the azimuthal angle of the C1'-H1' vector or, in other words, of the average structure (tilt, propeller twist, buckle, roll, χ angle) of each nucleotide along the sequence. The small variations of spin-lattice relaxation rates between the three central thymines may reflect these correlated motions. In order to complete our analysis, a careful study of these variations in each nucleotide in a labeled non-selfcomplementary undecamer is presently being carried out in our laboratory.

References

Abragam, A. (1961) *The Principles of Nuclear Magnetism*, Oxford University Press, Oxford.

Borer, P.N., LaPlante, S.R., Kumar, A., Zanatta, N., Martin, A., Hakkinen, A. and Levy, G.C. (1994) *Biochemistry*, **33**, 2441–2450.

Boyd, J., Hommel, U. and Campbell, I.D. (1990) *Chem. Phys. Lett.*, **175**, 477–483.

Briki, F., Ramstein, J., Lavery, R. and Genest, D. (1991) *J. Am. Chem. Soc.*, **113**, 2490–2493.

Briki, F. (1993) Ph.D. Thesis, University of Paris VI, Paris.

Briki, F. and Genest, D. (1993) *J. Biomol. Struct. Dyn.*, **11**, 43–56.

Brown, D.G., Sanderson, M.S., Garman, E. and Neidle, S. (1992) *J. Mol. Biol.*, **226**, 481–490.

Chanteloup, L. and Beau, J.M. (1992) *Tetrahedron Lett.*, **33**, 5347–5350.

Coll, M., Frederick, C.A., Wang, A.H.-J. and Rich, A. (1987) *Proc. Natl. Acad. Sci. USA*, **84**, 8385–8389.

Drew, H.R., Wing, R.M., Takano, T., Broka, C., Tanaka, S., Itakura, K. and Dickerson, R.E. (1981) *Proc. Natl. Acad. Sci. USA*, **78**, 2179–2183.

Early, T.A. and Kearns, D.R. (1979) *Proc. Natl. Acad. Sci. USA*, **76**, 4170–4174.

Edwards, K.J., Brown, D.G., Spink, N., Skelly, J.V. and Neidle, S. (1992) *J. Mol. Biol.*, **226**, 1161–1173.

Eimer, W., Williamson, J.R., Boxer, S.G. and Pecora, R. (1990) *Biochemistry*, **29**, 799–811.

Fratini, A.V., Kopka, M.L., Drew, H.R. and Dickerson, R.E. (1982) *J. Biol. Chem.*, **257**, 14686–14707.

Genest, D. and Wahl, P.L. (1978) *Biochim. Biophys. Acta*, **521**, 502–509.

Gueron, M., Kochoyan, M. and Leroy, J.L. (1987) *Nature*, **328**, 89–92.

Hogan, M.E. and Jardetzky, O. (1979) *Proc. Natl. Acad. Sci. USA*, **76**, 6341–6345.

Hogan, M.E. and Jardetzky, O. (1980) *Biochemistry*, **19**, 3460–3468.

Janes, N., Ganapathy, S. and Oldfield, E. (1983) *J. Magn. Reson.*, **54**, 111–121.

Kay, L.E., Nicholson, L.K., Delaglio, F., Bax, A. and Torchia, D.A. (1992) *J. Magn. Reson.*, **97**, 359–375.

Keepers, J.W. and James, T.L. (1982) *J. Am. Chem. Soc.*, **104**, 929–939.

Koning, T.M.G., Boelens, R., Van der Marel, G.A., Van Boom, J.H. and Kaptein, R. (1991) *Biochemistry*, **30**, 3787–3797.

Lancelot, G. (1977) *Biochimie*, **59**, 587–596.

Lancelot, G., Chanteloup, L., Beau, J.M. and Thuong, N.T. (1993a) *J. Am. Chem. Soc.*, **115**, 1599–1600.

Lancelot, G., Chanteloup, L., Beau, J.M. and Thuong, N.T. (1993b) *J. Am. Chem. Soc.*, **115**, 5891.

Leroy, J.L., Broseta, D. and Gueron, M. (1985) *J. Mol. Biol.*, **124**, 165–178.

Lipari, G. and Szabo, A. (1982a) *J. Am. Chem. Soc.*, **104**, 4546–4559.

Lipari, G. and Szabo, A. (1982b) *J. Am. Chem. Soc.*, **104**, 4559–4570.

McConnell, K.J., Nirmala, R., Young, M.A., Ravishanker, G. and Beveridge, D.L. (1994) *J. Am. Chem. Soc.*, **116**, 4461–4462.

Naito, A., Ganapathy, S., Raghunathan, P. and McDowell, C.A. (1983) *J. Chem. Phys.*, **79**, 4173–4182.

Palmer, A.G., Rance, M. and Wright, P.E. (1991) *J. Am. Chem. Soc.*, **113**, 4372–4380.

Pelton, J.G. and Wemmer, D.E. (1989) *Proc. Natl. Acad. Sci. USA*, **86**, 5723–5727.

Peng, J.W., Thanabal, V. and Wagner, G. (1991) *J. Magn. Reson.*, **94**, 82–100.

Peng, J.W. and Wagner, G. (1992) *J. Magn. Reson.*, **98**, 308–332.

Pines, A., Gibby, M.G. and Waugh, J.S. (1972) *Chem. Phys. Lett.*, **15**, 373–376.

Robins, M.J., Wilson, J.S. and Hanske, F. (1983) *J. Am. Chem. Soc.*, **105**, 4059–4065.

Rose, M.E. (1957) *Elementary Theory of Angular Momentum*, Wiley, New York, NY.

Saenger, W. (1984) *Principles of Nucleic Acid Structure*, Springer, New York, NY.

Schmitz, U., Kumar, A. and James, T.L. (1992) *J. Am. Chem. Soc.*, **114**, 10654–10656.

Schurr, J.M. and Fujimoto, B.S. (1988) *Biopolymers*, **27**, 1543–1569.

Sinha, N.D., Biernat, J. and Köster, H. (1983) *Tetrahedron Lett.*, **24**, 5843–5846.

Swaminathan, S., Ravishanker, G. and Beveridge, D.L. (1991) *J. Am. Chem. Soc.*, **113**, 5027–5040.

Tabernero, L., Verdaguer, N., Coll, M., Fita, I., Van der Marel, G.A., Van Boom, J.H., Rich, A. and Aymami, J. (1993) *Biochemistry*, **32**, 8403–8410.

Tirado, M.M. and Garcia de la Torre, J. (1979) *J. Chem. Phys.*, **71**, 2581–2587.

Tirado, M. M. and Garcia de la Torre, J. (1980) *J. Chem. Phys.*, **73**, 1986–1993.

Vega, M.C., Garcia Saez, I., Aymami, J., Eritja, R., Van der Marel, G.A., Van Boom, J.H., Rich, A. and Coll, M. (1994) *Eur. J. Biochem.*, **222**, 721–726.

Vorbrüggen, H., Krolikiewicz, K. and Bennua, B. (1981) *Chem. Ber.*, **114**, 1234–1255.

Withka, J.M., Swaminathan, S., Srinivasan, J., Beveridge, D.L. and Bolton, P.H. (1992) *Science*, **255**, 597–599.

Wittebort, R.J. and Szabo, A. (1978) *J. Chem. Phys.*, **69**, 1722–1736.

Wüthrich, K. (1986) *NMR of Proteins and Nucleic Acids*, Wiley, New York, NY.